ACS OMEGA

Article

Cite This: ACS Omega 2020, 5, 791−798

http://pubs.acs.org/journal/acsodf

Ti-Doped SBA-15 Catalysts Used in Phenol Oxidation Reactions

Ghadeer Almohammadi, Colin O'Modhrain, Sean Kelly,† and James A. Sullivan*

UCD School of Chemistry, Belfield, Dublin 4, Ireland

ABSTRACT: Two Ti-SBA-15 catalysts are synthesized using techniques that should either deposit Ti atoms specifically at the SBA-15 surface or allow Ti-containing species to exist at both the surface and within the bulk of SBA-15. The materials have been characterized by Fourier transform infrared (FTIR), Raman and UV visible spectroscopies, transmission electron microscopy, scanning electron microscopy/energy-dispersive X-ray spectrometry microscopies, and N_2 physisorption experiments. They have been applied in the total oxidation of phenol under catalytic wet air oxidation (CWAO) conditions and using photo- and plasma promotion. The materials retain the structure of SBA-15 following the doping in both cases and Ti incorporation is confirmed. The nature of the incorporated Ti remains unclear—with evidence for anatase TiO_2 (from Raman and UV vis analysis) and evidence for atomically dispersed Ti from FTIR. In terms of reactivity, the presence of Ti in the in situ-prepared catalyst improves reactivity in the photopromoted reaction (increasing conversion from 28 to 60%), while both Ti catalysts improve reactivity in the CWAO reaction (by 7% over the in situ catalyst and by 25% over the grafted material). The presence of Ti has no beneficial effect on conversion in the plasma-promoted reaction. Here, however, Ti does affect the nature of the oxidized intermediates formed during the total phenol oxidation.

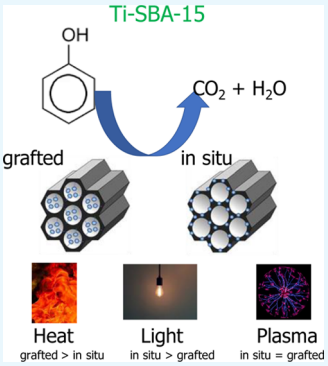

1. INTRODUCTION

Since their discovery, mesoporous materials have generated a significant amount of research interest with potential uses as adsorbents, chromatographic materials, catalysts, and catalyst supports.[1−4] The ease with which mesoporous SiO_2 materials can be modified (either post-preparation or during preparation) has expanded these interests to include the study of tethered homogeneous catalysts and atomically dispersed catalysts.[5−8]

In this work, we study Ti-modified SBA-15 materials as catalysts in the total oxidation of aqueous phenol (a model pollutant). Ti-SBA catalysts have been used in a range of different selective and total oxidation reactions,[9−15] and previously, we have been interested in Ti-modified mesoporous SiO_2 materials as catalysts in alkene selective oxidation reactions.[16]

Solid-phase materials have also long been studied as catalysts for the total oxidation of a range of aqueous phase pollutants using several advanced oxidation techniques including catalytic wet air oxidation (CWAO),[17] photocatalysis,[18] and more recently, plasma-promoted reactions.[19] In respect of this work, Ti-modified SBA-15 (with and without further modification) has been used in the photocatalytic oxidation of phenol and other model pollutants.[20−24] Within these, Jiang et al.[20] have used a one-pot hydrothermal synthesis (equivalent to one of our syntheses below), while Ryczkowski at al.[21] used far higher concentrations of Ti following a surface deposition. Both report anatase TiO_2 formation and use UV light promotion (while we use visible light in this work).

Regarding CWAO of phenol, there has been significantly more work (albeit on different catalysts), Luck produced a significant review[25] in 1999; more recent work has concentrated upon supported noble and non-noble metallic and oxide systems.[26−30]

In this contribution, we look at the total oxidation of phenol (a model aqueous pollutant) over two types of Ti-modified SBA-15 materials studying their reactivity using CWAO, photocatalysis, and plasma-promoted techniques. The types of Ti-SBA-15 prepared differ in the supposed location of the Ti atoms in/on the materials. In one preparation, Ti atoms are grafted to the surface of a pre-prepared SBA-15 material (meaning the Ti atoms should be only available at the surface of the final composite), and in the second, Ti atoms are included in the SBA-15 preparation mixture (meaning that theoretically Ti atoms should be available at the surface of the materials and should also be present in the sub-surface "walls" of the modified SBA-15). To our knowledge, these (or analogous) materials have not previously been studied in catalyzed CWAO or plasma-promoted reactions.

2. RESULTS AND DISCUSSION

2.1. Catalyst Characterization. The catalysts were characteried using a number of techniques to confirm Ti incorporation and to attempt to determine the nature of the Ti-containing species.

Table 1 shows the principal results of the N_2 physisorption experiments collected from the parent SBA-15 material and both Ti-modified analogues. All materials exhibit a type IV isotherm with type H_1 desorption hysteresis loops (results not shown). H_1 loops arise from physisorption analysis of a rigid

Received: October 22, 2019
Accepted: December 5, 2019
Published: December 30, 2019

Table 1. BET Surface Areas and Average Pore Sizes of the Materials Determined from N_2 Physisorption

	% Ti	S_{BET} (m^2 g^{-1})	pore size (nm)
SBA-15	0	601	5.0
Ti-SBA-15 (grafted)	2.5	502	5.3
Ti-SBA-15 (in situ)	1.9	924	6.0

mesopore structure, suggesting that these structures contain pores that have a narrow size distribution range. The parent SBA-15 material had a surface area of 601 m^2 g^{-1} (with an average pore size of 5.30 nm). Grafting Ti to the surface decreased the surface area to 502 m^2 g^{-1} (without altering the average pore size), while inclusion of Ti within the catalyst preparation mixture resulted in the formation of a material with a far higher surface area (924 m^2 g^{-1}) and a slightly decreased BJH-derived average pore size (5.00 nm). This suggests that the addition of Ti to the condensing SBA-15 mixture may have hindered SiO_2 condensation (e.g., by preventing the condensation of SiO_2 onto Ti sites) and thus decreased wall thickness and increased Brunauer–Emmett–Teller (BET) surface area of the final condensed material.

Figure 1 shows the TEM micrographs collected from each material and again, it is clear in all cases that the porous structure of the SBA-15 parent material is retained following both the post-preparation grafting of Ti to the surface and the inclusion of Ti into the SBA-15 preparation mixture. An analysis of the channel size from the TEM suggests that the SBA-15 material's channels are ∼4.9 nm and that this falls somewhat when Ti is grafted to the surface (to ∼4.5 nm) and increases to ∼6 nm when Ti is included in the SBA-15 preparation mixture (again suggesting thinner walls). There is no evidence for particulate TiO_2 in any of the TEM images. Interestingly, attempts to prepare (using the in situ process) an SBA-15 sample which had twice the loading that we have used here result in the precipitated material having no such porous structure (suggesting there is a limit to how much Ti can be incorporated into the materials without preventing the formation of the mesoporous structure); scanning electron microscopy (SEM) images (Figure 2) show that all three materials have a rodlike topography, while energy-dispersive X-ray spectrometry (EDX) analysis confirms the presence of Si and O in the SBA-15 samples and confirms the presence of Ti in the mixed oxide materials. The levels of Ti in the Ti SBA-15 (in situ) sample are measured at ∼7.3%. This is far higher than the 1.9% expected and suggests that some SiO_2 precursors had not crystallized from the solution during the preparation. Conversely, EDX measurement of the Ti levels in the grafted material was (at 1.1%) lower than the expected 2.5%.

Figure 3 shows the UV visible spectra of the materials and, from this, it is clear that both Ti-containing materials have semiconductor-like properties (both absorbing UV light), while SBA-15 is an insulator. Both the Ti-SBA-15 (grafted) and the Ti-SBA-15 (in situ) show absorbance edges reminiscent of semiconductors with the latter sample's absorption edge beginning at ∼380 nm and the former's at ∼350 nm. Band gap calculations (based on the assumption of anatase TiO_2)[38] suggest a band gap of 3.37 eV for the (in situ) material and one of 3.61 eV for the (grafted) analogue. Both of these are higher than the band gap of anatase TiO_2 which is 3.20 eV, and this is not unexpected for TiO_2/SiO_2 mixed oxides.[38,39] The band gap is also higher than that reported for the rutile structure (3.0 eV). However, this result does suggest the formation of a TiO_2 phase in either material is not ruled out.

Displaced Raman spectra (Figure 4) also suggest the formation of anatase TiO_2 domains in both of the Ti-containing materials. Interestingly, the Raman spectrometer used SiO_2 samples fluoresce following excitation with the 785 nm laser (meaning that spectra cannot be collected). However, the incorporation of minor amounts of titanium in these samples sufficiently quench this fluorescence and spectra can be collected.

For both types of synthesis procedures, samples analyzed by Raman spectroscopy showed features at 147, 395, 518, and 640 cm^{-1}, which are characteristic of anatase-phase TiO_2.[40]

This was unexpected, suggesting that the Ti is not (as we would have hoped) atomically dispersed but rather (at least for a portion of the Ti atoms) present as TiO_2. Also, the intensity of all of the TiO_2-related peaks increases as the nominal levels of Ti within the samples increases. This is true for both types of preparation (results not shown). No peaks relating to the rutile TiO_2 structure were noted.

Figure 5 shows the Fourier transform infrared (FTIR) spectra of the three samples of interest. The spectrum of SBA-15 is as expected.[41] Sharp IR peaks at 3750 cm^{-1} are attributed to the vibration of isolated surface silanol groups. The broad band centered at 3440 cm^{-1} relates to surface silanols that are undergoing hydrogen bonding with other silonal groups or with physisorbed water. The peaks at 1640 cm^{-1} related to the bend of adsorbed H_2O molecules. Characteristic Si–O–Si bends appear at ∼1330 and 820 cm^{-1}, which confirmed the formation of a condensed silica network.[42]

The FTIR spectrum of the Ti-SBA-15 (grafted) material differs from this in several ways. First, the intensity of the isolated silanol peaks at 3750 cm^{-1} is significantly lower (confirming condensation of Ti-isopropoxide to these sites). Secondly, a band appears at ∼970 cm^{-1} (see the inset) which relates to asymmetric stretching of the Si–O–Ti framework[43]

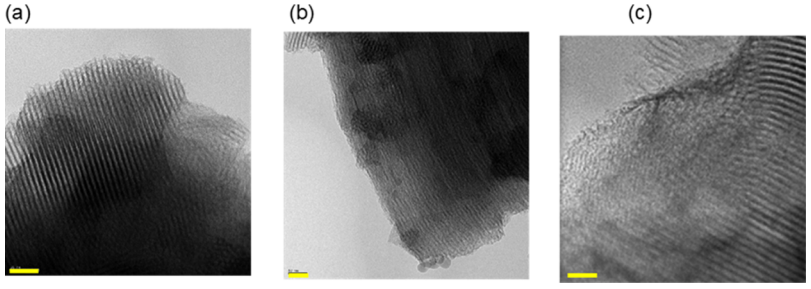

Figure 1. TEM images of unmodified (a) SBA-15, (b) Ti-SBA-15 (grafted), and (c) Ti-SBA-15 (in situ). Scale bars are 50 nm.

DOI: 10.1021/acsomega.9b03530
ACS Omega 2020, 5, 791–798

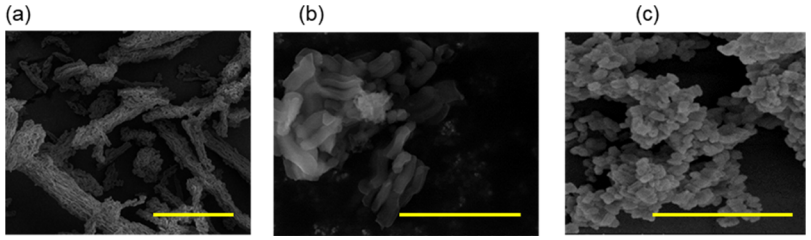

Figure 2. SEM images of unmodified (a) SBA-15 (scale 50 μm), (b) Ti-SBA-15 (scale 5 μm) (grafted), and (c) Ti-SBA-15 (in situ) (scale 10 μm).

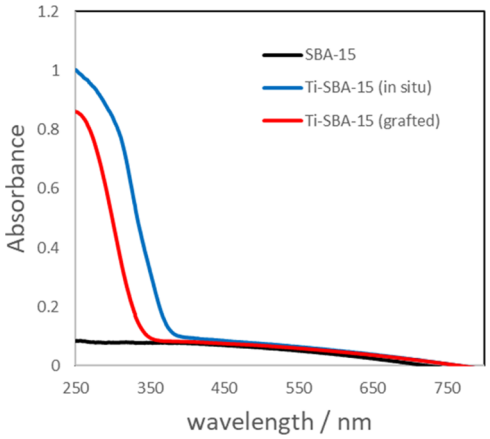

Figure 3. UV visible spectra of SBA-15, Ti-SBA-15 (grafted), and Ti-SBA-15 (in situ).

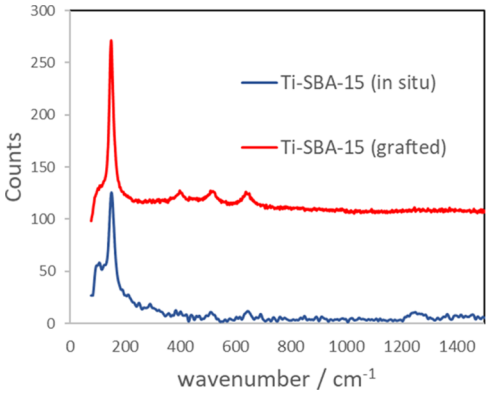

Figure 4. Displaced Raman spectra of Ti-SBA-15 (grafted) and Ti-SBA-15 (in situ) materials.

(which confirms the inclusion of Ti atoms onto the structure), and finally, the broad band at 3400 cm^{-1}, and the peak at 1650 cm^{-1} is significantly more intense than they were in the SBA-15 spectrum. These peaks indirectly and directly relate to adsorbed H_2O (suggesting that the Ti-modified material is more hydrophilic than the unmodified SBA-15 material).

The FTIR spectrum of the Ti-SBA-15 (in situ) material is shown in blue, and in this spectrum, it is clear that the peak relating to the isolated Si−OH species is significantly more intense than that in the spectrum of the grafted material (expected) and the unmodified material (unexpected). We ascribe this to the increased surface area in this material (thereby more isolated surface OH groups are present). Again, all of the expected Si−O−Si peaks are present, and again, a new peak (confirming Si−O−Ti) is seen at ∼950 cm^{-1}, and the water-related peaks (3400, 1650 cm^{-1}) are more intense than in the SBA-15 spectrum (suggesting the material is more

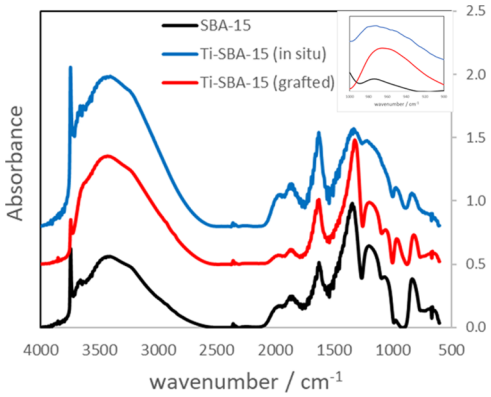

Figure 5. Displaced FTIR spectra of SBA-15, Ti-SBA-15 (grafted), and Ti-SBA-15 (in situ). The inset shows Si−O−Ti vibrations in the latter two samples.

hydrophilic than SBA-15). Interestingly TGA analysis also suggests this is the case. No peaks relating to surface Ti−OH can be seen in either spectrum of the Ti-modified materials.

The microscopic, spectroscopic, and physisorption characterizations of these materials matches those found previously for similarly prepared SBA-15 and Ti-modified SBA-15 materials.[31,33,34]

2.2. Catalytic Reactivity. The catalysts were applied in the probe phenol total oxidation reaction, where the catalysts were used in combination with heat (CWAO-type conditions) light (in a photocatalytic reaction) and in the presence of a plasma in order to evaluate (a) whether they were effective in the different reactions and (b) whether the location or nature of the Ti affected activity or selectivity.

Figure 6a shows the phenol conversions from the thermally promoted reaction (after 24 h) in the absence of the catalyst over SBA-15 and over the two Ti-modified analogues. Figure 7 and 8 show the results from the photocatalytic (24 h) and plasma-promoted reactions (10 min), respectively.

Regarding the CWAO reaction, there is a level of phenol conversion (∼15%) in the absence of catalysts and this increases to ∼22% in the presence of SBA-15. The conversion is further increased by the presence of both Ti-SBA-15 (grafted) and Ti-SBA-15 (in situ) catalysts with the (grafted) catalyst being the more active of the two with ∼47% compared to ∼30% phenol conversion after 24 h.

Figure 6b shows the levels of oxidized intermediates after 16 h of reaction over SBA-15 and both Ti-containing catalysts. Hydroquinine and benzoquinone were produced in all reactions (and in the absence of a catalyst), while interestingly, catechol was not formed. Levels of these within the mixture fell after 16 h (presumably due to further oxidation) and never got above a combined total of 12% within any the reaction mixtures. SBA-15 formed hydroquinone rather than benzoqui-

DOI: 10.1021/acsomega.9b03530
ACS Omega 2020, 5, 791−798

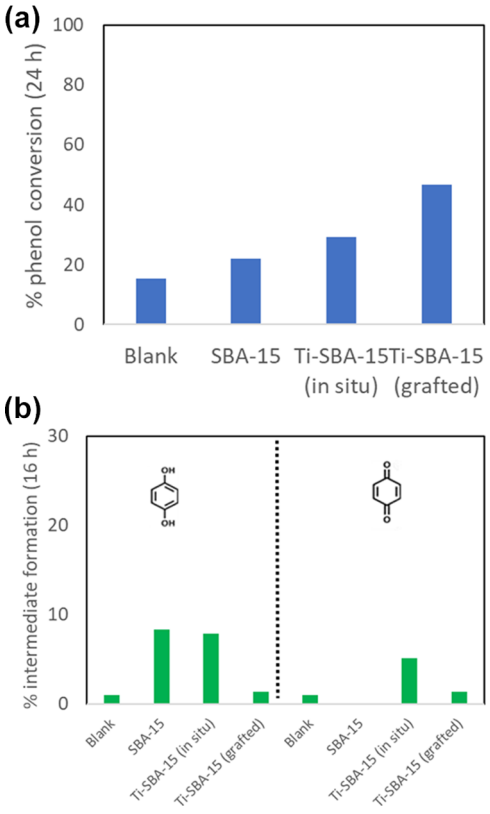

Figure 6. (a) Phenol conversion over the different catalysts in the CWAO reaction (24 h) and (b) levels of hydroquinone and benzoquinone intermediates formed during this reaction after 16 h.

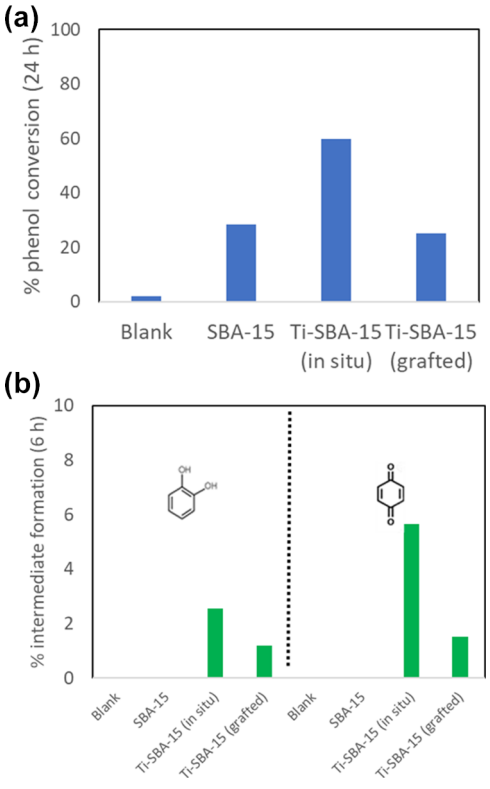

Figure 7. (a) Phenol conversion over the different catalysts in the photocatalyzed reaction (24 h) and (b) levels of catechol and benzoquinone intermediates formed during this reaction after 6 h.

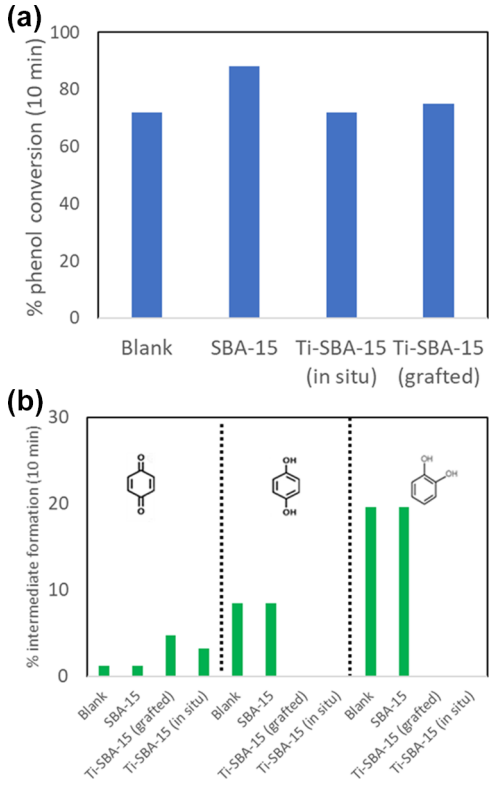

Figure 8. (a) Phenol conversion over the different catalysts in the plasma-promoted reaction (10 min), (b) levels of hydroquinone, catechol, and benzoquinone intermediates formed during this reaction.

none and, of the Ti-containing catalysts, the (in situ) material produced higher levels of hydroquinone and benzoquinone intermediates than the (grafted) material.

Figure 7a,b shows the same data (following 24 h reaction) from the photocatalytic reaction in the absence of catalysts, the presence of SBA-15, and the presence of both Ti-modified SBA-15 materials.

In these reactions, the conversion of phenol in the absence of catalysts is significantly lower than in the CWAO reactions above (with ∼2% conversion), while the presence of SBA-15 results in ∼28% conversion.

Regarding the Ti-containing materials, in contrast to the CWAO reaction above, the (in situ) catalyst was more reactive than the grafted material with the former converting ∼60% of the phenol and the latter converting ∼25%, which is a lower conversion than yielded by SBA-15 alone.

This reactivity is unexpected for several reasons, not least the fact that the catalysts here do not absorb the wavelengths of light that the solar simulator emits (see Figure 3), and SBA-15 is not known to have shown photoreactivity. This suggests that the mechanism of the reaction involved light absorption by a catalyst/reactant couple rather than the traditional electron/hole generation involved in semiconductor photocatalysis.

In any case, the reactivities of the Ti-containing materials are reversed when compared to the conversions on the CWAO reaction, where grafted was more reactive than the in situ materials.

Further interesting outcomes from these reactions are presented in Figure 8b, where the oxidized phenol intermediates generated following 6 h of photoreaction are shown. No intermediates are formed during the reactions in

DOI: 10.1021/acsomega.9b03530
ACS Omega 2020, 5, 791−798

the absence of catalysts or in the reactions over the unmodified SBA-15 material. Catechol and benzoquinone were formed over both Ti-modified materials (while hydroquinone was not). In general, more benzoquinone was produced. An aspect of interest here is the difference in intermediates formed during this reaction compared to those formed during the CWAO reaction above (where catechol was not formed and hydroquinone was) over both Ti-containing materials. This confirms that the reaction mechanism in both reactions of the conversion of phenol differs.

Figure 8 shows the phenol conversion following 10 min of exposure to plasma in the absence of catalysts and in the presence of SBA-15 and the two Ti-containing materials. Clearly, a catalyst is not required to achieve significant phenol conversions in these reactions with the reaction in the absence of the catalyst showing 72% conversion and that in the presence of unmodified SBA-15 showing a conversion of 88%.

The incorporation of Ti into (or onto) the SBA-15 catalyst results in decreased conversion relative to this (with conversions between 72 and 75%). It is clear that the effect of the presence of the plasma discharge and the resultant generation and utilization of the oxidizing aqueous $OH^{\bullet}$ radicals takes place in the liquid phase rather than on the catalyst. The most interesting effect of the Ti-containing materials in this reaction arises when the levels of oxidized intermediates following the reaction are considered. These are shown in Figure 8b. In a difference to the photocatalysis and CWAO reactions shown above, all three oxidized phenol intermediates (hydroquinone, benzoquinone, and catechol) are seen following these reactions.

In the reaction in the absence of the catalyst and in the reaction in the presence of unmodified SBA-15, all three intermediates are measured, following the 10 min reaction. In these cases, catechol was the most prevalent (at levels of ∼20% when formed) followed by hydroquinone (at ∼10%) and benzoquinone (at levels <5%).

In the presence of the Ti-containing materials, measurable levels of the former two intermediates (catechol and hydroquinone) are not seen, and the only measurable intermediate is benzoquinone (at levels of ∼5%). Given the phenol oxidation apparently happens in the aqueous phase (see conversions in the absence of the catalyst); this result suggests that the hydroquinone and catechol intermediates formed are further oxidized over the Ti-containing materials.

The different reactivities of the different materials under the different reaction conditions all point to different mechanisms of reaction in each case. In the case of the CWAO reaction, it would be expected that both surface-mediated oxidations and generated hydroxyl radicals can play a role.

Conversely, in the case of the photocatalyzed reactions, it would be expected that the actual oxidations would be carried out by OH radicals created either by reduction of water using promoted electrons (co-generating OH^- ions) or hole neutralizations, where a valence band hole would extract electrons from an adsorbed phenol molecule or from water (generating oxidizing OH radicals). For this reason, it would be expected that the mechanisms of these reactions should be similar to those of the plasma promoted reactions, where hydroxyl radicals and other radicals would be generated within the plasma (albeit with far greater concentrations of oxidants in the latter—resulting in the observed far faster reactions).

3. CONCLUSIONS

We have prepared and characterized 2 Ti-containing SBA-15 materials and applied them in the oxidation of aqueous phase phenol under thermal-, photo-, and plasma promotion.

One technique selectively placed Ti atoms on the SBA-15 surface (albeit the external surface and the surface within the mesopores), while the second technique should have resulted in Ti atoms both on the external surfaces and within the SiO_2 matrix.

Both techniques successfully incorporated Ti into or onto the SBA-15 material, and this is confirmed by EDX, UV vis, Raman, and FTIR spectroscopy. UV vis spectroscopy also suggested that the composite materials were semiconductors and Raman spectroscopy suggested anatase formation. TEM and BET analysis confirm that the porous structure of SBA-15 remained following incorporation of Ti, but the materials formed using the (in situ) Ti incorporation technique had a significantly higher surface area (which suggests that the presence of Ti in the SiO_2 matrix decreases the levels of further SiO_2 condensation).

Regarding the reactivity in the promotion of aqueous phenol oxidation, the (grafted) material was more active in the CWAO reaction, while the (in situ) sample was more active in the photocatalysis reaction, while reactivity of the two materials was equivalent in the plasma-promoted reaction (and lower than the reactivity of SBA-15 under the same conditions). The three types of reaction generated different collections of intermediates (catechol, hydroquinone, and benzoquinone), reflecting the fact that different reaction mechanisms must be in operation in operation in each oxidation process, and interestingly, in the plasma-promoted reaction, the main effect of Ti incorporation was to decrease the eventual levels of formation of these intermediates.

4. EXPERIMENTAL SECTION

4.1. Catalyst Preparation. *4.1.1. Synthesis of Mesoporous silica[31] (SBA-15).* P123 (4 g, 0.705 mmol, Sigma-Aldrich 99.99%) was added to a round-bottom flask (RBF) with HCl (120 mL, 2 M, Sigma-Aldrich 37% solution) and distilled H_2O (30 mL). The solution was stirred at room temperature until clear and homogenous. The reaction temperature was raised to 40 °C, and TEOS (8.5 g, 9.11 mL, 0.0408 mol, Sigma-Aldrich >99%) was added. The solution was then stirred for 20 h. After this time, the reaction mixture was aged under static conditions at 80 °C for 24 h. The resulting white precipitate was filtered under vacuum and washed with distilled H_2O (2 L). The solid was then dried at 80 °C, followed by calcination at 600 °C for 6 h. Thermogravimetric analysis of this material post-calcination suggested a surface hydroxyl concentration of 1.48 OH nm^2.[32]

4.1.2. Surface Modification of SBA-15. This process was a modification of the preparations discussed by Ahn et al.[33] SBA-15 (0.5 g, 8.32 mmol) was weighed into a pre-dried RBF. Dry ethanol (15 mL) was added with 78 μL titanium isopropoxide [$Ti(OiPr)_4$], (Aldrich, 97%). The reaction mixture was stirred under ambient conditions for 8 h to allow the condensation reaction to proceed to completion. The mixture was then filtered, and the solid was washed with dry ethanol (20 mL, Fischer 99.99%). The resulting white solid (which should nominally have ∼2.5% Ti assuming complete uptake) was dried overnight at room temperature prior to calcination at 550

DOI: 10.1021/acsomega.9b03530
ACS Omega 2020, 5, 791−798

°C for 5 h. This sample is called Ti-SBA-15 (grafted) in the text.

For the other Ti-loaded sample, the preparation was as follows:[34] P123 (3 g) was dissolved in 140 mL of deionized water in a 500 mL round-bottomed flask. The solution was stirred at 35 °C for 4 h. $TiCl_4$ (1 mmol, Sigma-Aldrich 99%) and (8.5 g, 9.11 mL, 0.0408 mol) of tetraethyl orthosilicate were added, and this mixture was continuously stirred at 35 °C. After stirring for 24 h, the resultant mixture was transferred into a Teflon-lined autoclave and aged at 100 °C for another 24 h without stirring. This reaction resulted in the precipitation of a solid-phase Ti-containing SiO_2 material. The solid was then filtered under vacuum, washed with deionized water, (×2) and absolute ethanol (×2) and dried in air at 100 °C for 12 h. The as-prepared products were then calcined in air at 550 °C for 5 h to oxidize and remove the template. This catalyst has a nominal Ti loading of ∼1.9% and is referred to as Ti-SBA-15 (in situ) in the text.

4.2. Catalyst Characterization. N_2 physisorption was carried out using Micromeritics ASAP 2020 Plus at a liquid N_2 boiling point (−196 °C), using N_2 as the inert probe; the collected data were fit using both BET and Barrett−Joyner−Halenda analyses to yield surface areas and pore sizes. BET analysis was carried out using Micromeritics ASAP 2020 Plus at a temperature of 77 K, using N_2 as the inert probe. In a typical BET experiment, approximately 100 mg of the sample was weighed and transferred to a glass bulb. A glass rod was then inserted into the bulb to reduce free space, and the bulb was reweighed. The bulb was then degassed at 350 °C for 4 h. Prior to analysis, the degassed bulb and sample were reweighed, with the resulting mass used in subsequent calculations. The adsorption and desorption of N_2 onto the sample was then monitored over the range of $0.05 < p/p_0 < 0.98$.

A Tecnai 20 Transmittance Electron Microscope (TEM) was used to image the materials. To prepare the samples for analysis, a spatula tip (∼1 mg) of sample was dispersed in isopropanol (10 mL). This mixture was sonicated for 10 min, and the resulting suspension (10 μL) was placed on a copper TEM mesh (Agar Scientific) and allowed to dry. The mesh was then placed in the TEM sample holder and introduced to the TEM via a side entry goniometer stage.

A Hitachi S5500 field emission scanning electron microscope was used to obtain SEM images of the materials. Prior to examination, 1−5 mg of the sample was mounted on an aluminum stub, which had been previously coated with a disposable carbon tab. The stub was then placed in a sample holder and loaded into the high-vacuum SEM chamber. The electron gun of the instrument was operated at an accelerating voltage of 20 kV under high vacuum. This instrument was also used to collect EDX spectra of the samples.

Raman spectra were collected using a Senterra III Raman scope (Bruker); the spectrometer was fitted with a confocal microscope (Olympus BX with 20× and 50× magnification lenses). A laser wavelength of 785 nm operated at 100 mW was used as the Raman excitation source, and a germanium thermoelectrically cooled charged couple device (Androf) was used as a detector. The aperture was set to 50 μm for experiments.[35]

A Bruker VERTEX 70 FTIR spectrometer was used for infrared analysis of the materials. Liquid N_2 was used to cool the Mercury−Cadmium−Telluride detector prior to scanning. The range scanned was between 600 and 4000 cm^{-1}, with the final spectrum resulting from an average of 32 scans. Approximately, 10 mg of the sample was used for each analysis.

UV visible spectra were collected using a Jasco V-650 spectrometer equipped with an integrating sphere (ISV-722). A twin source, deuterium and halogen lamp was used, and the instrument was set in the absorbance mode with a range between 250 and 850 nm. Data points were recorded at intervals of 0.2 nm, with the UV−vis bandwidth set to 5 nm with a medium response rate and a scan rate of 200 nm per minute. In a typical experiment, 100 mg of the recoverable sample was required. Prior to the sample analysis, a background spectrum was recorded using a white board which was used for baseline correction of the spectra obtained.

To calculate the band gap energy of TiO_2-type semiconducting materials, a Tauc plot of $(\alpha h\nu)^2$ against $h\nu$ must be produced,[36] where α is the absorbance value corresponding to the photon energy, $h\nu$, in electron volts (eV). From this plot, a linear equation is obtained from which the slope and intercept can be extrapolated. These values are used to calculate the band gap in electron volts (eV).[37]

4.2.1. Reactivity Studies. The reactivity of the SBA-15 material and both modified Ti-SBA-15 materials were analyzed in the total oxidation of phenol under three types of reaction, that is, CWAO, photocatalysis, and plasma promotion. In all cases, the catalyst mass was 10 mg, and the phenol concentration was 100 ppm with a volume of 10 mL.

4.2.2. Catalytic Wet Air Oxidation. A known amount of the catalyst material was added to a Teflon liner (20 mL) with phenol solution (10 mL). The liner was placed in a stainless-steel autoclave in a furnace. The autoclave was heated to 150 °C at a rate of 20 °C min^{-1} and held at this temperature for a set amount of time (0, 6, 16, 20, and 24 h). Following this, the Teflon cup was cooled to room temperature using an ice bath. The solution within was separated from the catalyst by centrifugation (13 000 rpm, 1 min), and the supernatant was extracted to a high-performance liquid chromatography (HPLC) vial for analysis, and the catalyst pellet was retained for post-reaction characterization.

4.2.3. Photocatalysis. All photocatalytic studies were carried out using an Atlas SuntestTM CPS+ instrument and externally irradiated by a 300 W Xe lamp. A filter was applied to the emitted light, resulting in incident light on the reaction vessels lying in the visible region of the electromagnetic spectrum (400−700 nm). This chamber was maintained at room temperature for the duration of the experiment, as measured using an internal thermometer. In a typical photopromoted reaction setup, a known amount of the catalyst was added to a tall screw neck vial (20 mL). Phenol solution was contacted with the catalyst, and the vessel was immediately placed in a vial holder in the solar chamber. Once the reaction had begun, samples were removed at preset intervals (0, 6, 16, 20, and 24 h) over a period of 24 h. Phenol loss through evaporation was prevented by sealing the reaction vessels. The samples were extracted and separated by centrifugation (13 000 rpm, 1 min). The resulting supernatant was transferred to a HPLC vial for analysis.

4.2.4. Plasma Promotion. A gas phase discharge reactor with the liquid acting as an electrode was used for these studies. This design was chosen because of its ease of setup and effective reproducibility. The distance between the pin electrode tip and the liquid surface remained constant throughout (5 mm).

DOI: 10.1021/acsomega.9b03530
ACS Omega 2020, 5, 791−798

The discharge setup was powered by a PVM500 resonant HV power supply (Information Unlimited). The plasma was produced by tuning the frequency for applied voltage to 60 kV and pulsed by a duty frequency controller with a duty cycle of 3 kHz.

For each experiment, phenol solution and catalyst were added to a long-neck vial. The vial was sonicated (30 s) to suspend the solid catalyst in solution. The resulting mixture was treated with the glow discharge plasma for a set period (1, 5, and 10 min), with a sample removed at the end of each period. The sample was centrifuged (13 000 rpm, 1 min), and the supernatant extracted to a HPLC vial for analysis.

Following the brief exposures to the atmospheric plasma stream described above, the temperature of each solution was much increased over room temperature (60−85 °C). To ensure that this change did not result in significant removal of phenol, tests were carried out to mimic the heating conditions within the plasma reactor. The results of this experiment showed that maximum phenol loss through evaporation was below 1.5% after 15 min.

For all reaction configurations, blank experiments in the absence of the catalyst were also carried out.

4.2.5. Reactant and product analysis. The liquid samples extracted to HPLC vials were analyzed using an Agilent 1200 series HPLC instrument equipped with an Agilent ZORBAX Eclipse XDB-C18 column (150 mm length × 4.6 mm diameter, 5 μm particle size). The eluates were analyzed using an online UV−vis detector. The total flow on the column was 1 mL min^{-1}, and the pressure was regulated to 80 bar. The mobile phase components (water, methanol, and acetic acid) were present in a 90:9:1 ratio.

For quantification, calibration curves of phenol and the intermediate oxidation products (catechol, hydroquinone, and benzoquinone) were produced under these conditions. No other partial oxidation products en route to CO_2 were noted. The detector was set to analyze the column eluant at 244 and 275 nm.

AUTHOR INFORMATION

Corresponding Author

*E-mail: james.sullivan@ucd.ie.

ORCID

James A. Sullivan: 0000-0002-3746-3047

Present Address

†Departement Chemie, Universiteit Antwerpen, Belgium.

Notes

The authors declare no competing financial interest.

ACKNOWLEDGMENTS

The KSA Ministry of Higher Education is acknowledged for providing G.A.'s studentship, and IRC funded the plasma work under grant ref: GOIPD/2017/1000.

REFERENCES

(1) Zhao, D.; Feng, J.; Huo, Q.; Melosh, N. Triblock copolymer syntheses of mesoporous silica with periodic 50 to 300 angstrom pores. *Science* **1998**, *279*, 548−552.

(2) Stöber, W.; Fink, A.; Bohn, E. Controlled growth of monodisperse silica spheres in the micron size range. *J. Colloid Interface Sci.* **1968**, *26*, 62−69.

(3) Trewyn, B. G.; Nieweg, J. A.; Zhao, Y.; Lin, V. S.-Y. Biocompatible mesoporous silica nanoparticles with different morphologies for animal cell membrane, penetration. *Chem. Eng. J.* **2008**, *137*, 23−29.

(4) Kokunešoski, M.; Gulicovski, J.; Matović, B.; Logar, M.; Milonjić, S. K.; Babić, B. Synthesis and Surface Characterization of Ordered Mesoporous Silica SBA-15. *Mater. Chem. Phys.* **2010**, *124*, 1248−1252.

(5) Van Der Voort, P.; Vercaemst, C.; Schaubroeck, D.; Verpoort, F. Ordered mesoporous materials at the beginning of the third millennium: new strategies to create hybrid and non-siliceous variants. *Phys. Chem. Chem. Phys.* **2008**, *10*, 347−360.

(6) Xu, W.; Yu, B.; Zhang, Y.; Chen, X.; Zhang, G.; Gao, Z. Single-site SBA-15 supported zirconium catalysts. Synthesis, characterization and toward cyanosilylation reaction. *Appl. Surf. Sci.* **2015**, *325*, 227−234.

(7) Chaudhary, V.; Sweta, D. Synthesis and Catalytic Performance of SBA-15 Supported Catalysts for Oxidation of Styrene. *Int. J. Sci. Eng. Res.* **2016**, *7*, 1743−1748.

(8) Morgan, G. G.; Fennell, K.; Kishore, M. J. L.; Sullivan, J. A. Tethering of Dinuclear Complexes to SBA-15 and Their Application in CO_2 Hydrogenation. *ChemCatChem* **2014**, *5*, 951−958.

(9) Wróblewska, A.; Makuch, E. The utilization of Ti-SBA-15 catalyst in the epoxidation of allylic alcohols. *React. Kinet., Mech. Catal.* **2012**, *105*, 451.

(10) Wu, P.; Tatsumi, T.; Komatsu, T.; Yashima, T. Postsynthesis, Characterization, and Catalytic Properties in Alkene Epoxidation of Hydrothermally Stable Mesoporous Ti-SBA-15. *Chem. Mater.* **2002**, *14*, 1657−1664.

(11) Sacaliuc, E.; Beale, A.; Weckhuysen, B.; Nijhuis, T. Propene epoxidation over Au/Ti-SBA-15 catalysts. *J. Catal.* **2007**, *248*, 235−248.

(12) Zhan, W.; Yao, J.; Xiao, Z.; Guo, Y.; Wang, Y.; Guo, Y.; Lu, G. Catalytic performance of Ti-SBA-15 prepared by chemical vapor deposition for propylene epoxidation: The effects of SBA-15 support and silylation. *Microporous Mesoporous Mater.* **2014**, *183*, 150−155.

(13) Kolev, H.; Todorova, S.; Naydenov, A.; Ene, R.; Ivanov, G.; Parvulescu, V.; Kadinov, G. Catalytic Activity of Mesoporous SBA-15 modified with Pt and Ti in a Deep Methane, n-hexane and CO Oxidation. *Athens J. Sci.* **2014**, *1*, 9−20.

(14) Venezia, A. M.; Di Carlo, G.; Liotta, L. F.; Pantaleo, G.; Kantcheva, M. Effect of Ti(IV) loading on CH_4 oxidation activity and SO_2 tolerance of Pd catalysts supported on silica SBA-15 and HMS. *Appl. Catal., B* **2011**, *106*, 529−539.

(15) Ye, W.; Lin, Z.; Dong, B.; Kang, J.; Zheng, X.; Wang, X. Preparation and Catalytic Properties of Ti-SBA-15 Mesoporous Materials. *Mater. Sci. Appl.* **2011**, *02*, 661−668.

(16) O'Callaghan, N.; Sullivan, J. A. Towards selective catalytic oxidations using in situ generated H_2O_2. *Appl. Catal., B* **2014**, *146*, 258−266.

(17) Pintar, A.; Levec, J. Catalytic Oxidation of Organics in Aqueous Solutions. *J. Catal.* **1992**, *135*, 345−357.

(18) Das, S. K.; Bhunia, M. K.; Bhaumik, A. Highly ordered Ti-SBA-15: Efficient H_2 adsorbent and photocatalyst for eco-toxic dye degradation. *J. Solid State Chem.* **2010**, *183*, 1326−1333.

(19) Cheng, H.-H.; Chen, S.-S.; Yoshizuka, K.; Chen, Y.-C. Degradation of phenolic compounds in water by non-thermal plasma treatment. *J. Water Chem. Technol.* **2012**, *34*, 179−189.

(20) Yang, L.; Jiang, Z.; Lai, S.; Jiang, C.; Zhong, H. Synthesis of Titanium Containing SBA-15 and Its Application for Photocatalytic Degradation of Phenol. *Int. J. Chem. Eng.* **2014**, *2014*, 691562.

(21) Olejnik, T.; Pasieczna-Patkowska, S.; Lesiuk, A.; Ryczkowski, J. Phenol and methylene blue photodegradation over Ti/SBA-15 materials under UV light. *Pol. J. Chem. Technol.* **2016**, *18*, 30−38.

(22) Li, G.; Zhao, X. S. Characterization and Photocatalytic Properties of Titanium-Containing Mesoporous SBA-15. *Ind. Eng. Chem. Res.* **2006**, *45*, 3569−3573.

(23) Yang, L.; Wang, B.; Lai, S.; Jiang, C.; Zhong, H. Enhancing photocatalytic degradation of phenol through nitrogen- and nitrogen/fluorine-codoped Ti-SBA-15. *RSC Adv.* **2015**, *5*, 53299−53305.

DOI: 10.1021/acsomega.9b03530
ACS Omega 2020, 5, 791−798

(24) Liu, F.; Yu, J.; Tu, G.; Qu, L.; Xiao, J.; Liu, Y.; Wang, L.; Lei, J.; Zhang, J. Carbon nitride coupled Ti-SBA15 catalyst for visible-light-driven photocatalytic reduction of Cr (VI) and the synergistic oxidation of phenol. *Appl. Catal., B* **2017**, *201*, 1−11.
(25) Luck, F. Wet air oxidation: past, present and future. *Catal. Today* **1998**, *53*, 81−91.
(26) Quintanilla, A.; Casas, J. A.; Rodriguez, J. J. Hydrogen peroxide-promoted-CWAO of phenol with activated carbon. *Appl. Catal., B* **2010**, *93*, 339−345.
(27) Arena, F.; Italiano, C.; Raneri, A.; Saja, C. Mechanistic and kinetic insights into the wet air oxidation of phenol with oxygen (CWAO) by homogeneous and heterogeneous transition-metal catalysts. *Appl. Catal., B* **2010**, *99*, 321−328.
(28) Baloyi, J.; Ntho, T.; Moma, J. Synthesis of highly active and stable Al/Zr pillared clay as catalyst for catalytic wet oxidation of phenol. *J. Porous Mater.* **2019**, *26*, 583−597.
(29) Guerra-Que, Z.; Pérez-Vidal, H.; Torres-Torres, G.; Arévalo-Pérez, J. C.; Silahua Pavón, A. A.; Cervantes-Uribe, A.; de los Monteros, A. E.; Lunagómez-Rocha, M. A. Treatment of phenol by catalytic wet air oxidation: a comparative study of copper and nickel supported on gamma-alumina, ceria and gamma-alumina-ceria. *RSC Adv.* **2019**, *9*, 8463−8479.
(30) Izquierdo-Colorado, A.; Torres-Torres, G.; Gamboa-Rodríguez, M. T.; Silahua-Pavón, A. A.; Arévalo-Pérez, J. C.; Cervantes-Uribe, A.; Cordero-García, A.; Beltramini, J. N. Catalytic Wet Air Oxidation (CWAO) of Phenol in a Fixed Bed Reactor Using Supported Ru and Ru-Au Catalysts: Effect of Gold and Ce Loading. *ChemistrySelect* **2019**, *4*, 1275−1284.
(31) Gutiérrez, O. Y.; Fuentes, G. A.; Salcedo, C.; Klimova, T. SBA-15 supports modified by Ti and Zr grafting for NiMo hydrodesulfurization catalysts. *Catal. Today* **2006**, *116*, 485−497.
(32) Mueller, R.; Kammler, H. K.; Wegner, K.; Pratsinis, S. E. OH surface density of SiO_2 and TiO_2 by thermogravimetric analysis. *Langmuir* **2003**, *19*, 160−165.
(33) Kim, M.-J.; Chang, S.-H.; Choi, J.-S.; Ahn, a. W.-S. Physicochemical properties of Ti-grafted SBA-15. *React.Kinet.Catal.-Lett.* **2004**, *82*, 27−32.
(34) Zhang, H.; Tang, C.; Lv, Y.; Gao, F.; Dong, L. Direct synthesis of Ti-SBA-15 in the self-generated acidic environment and its photodegradation of Rhodamine B. *J. Porous Mater.* **2014**, *21*, 63−70.
(35) Mulvaney, S. P.; Keating, C. D. Raman Spectroscopy. *Anal. Chem.* **2000**, *72*, 145−158.
(36) López, R.; Gómez, R. Band-gap energy estimation from diffuse reflectance measurements on sol−gel and commercial TiO_2: a comparative study. *J. Sol-Gel Sci. Technol.* **2012**, *61*, 1−7.
(37) Mayhar, A.; Behnajady, M. A.; Modirshahla, N. Characterisation and Photocatalytic Activity of TiO_2-SiO_2 mixed oxide nanoparticles prepared by sol-gel method. *Indian J. Chem., Sect. A: Inorg., Bio-inorg., Phys., Theor. Anal. Chem.* **2010**, *49*, 1593−1600.
(38) Anderson, C.; Bard, A. J. Improved Photocatalytic Activity and Characterization of Mixed TiO_2/SiO_2 and TiO_2/Al_2O_3 Materials. *J. Phys. Chem. B* **1997**, *101*, 2611−2616.
(39) Frank, O.; Zukalova, M.; Laskova, B.; Kürti, J.; Koltai, J.; Kavan, L. Raman spectra of titanium dioxide (anatase, rutile) with identified oxygen isotopes (16, 17, 18). *Phys. Chem. Chem. Phys.* **2012**, *14*, 14567−14572.
(40) Tadjarodi, A.; Jalalat, V. Synthesis and Characterization of Functionalized SBA-15 Mesoporous Silica by N, Ń-Bis(salicylidene)-ethylenediamine Schiff-Base. *J. North. Sci.* **2013**, *3*, 477−482.
(41) Appiah-Ntiamoah, R.; Chung, W.-J.; Kim, H. A highly selective SBA-15 supported fluorescent "turn-on" sensor for the fluoride anion. *New J. Chem.* **2015**, *39*, 5570−5579.
(42) Morey, M. S.; O'Brien, S.; Schwarz, S.; Stucky, G. D. Hydrothermal and Postsynthesis Surface Modification of Cubic, MCM-48, and Ultralarge Pore SBA-15 Mesoporous Silica with Titanium. *Chem. Mater.* **2000**, *12*, 898−911.
(43) Sanjinés, R.; Tang, H.; Berger, H.; Gozzo, F.; Margaritondo, G.; Lévy, F. Electronic Structure of Anatase TiO_2. *J. Appl. Phys.* **1994**, *75*, 2945−2951.

DOI: 10.1021/acsomega.9b03530
ACS Omega 2020, 5, 791−798